To be submitted to Journal of Climate

The extratropical linear step response to tropical precipitation anomalies and its use in constraining projected circulation changes under climate warming

Pranab Deb[1,3], Adrian J. Matthews[2], Manoj M. Joshi[3], Natasha Senior[3]

1 Centre for Oceans, Rivers, Atmosphere and Land Science (CORAL), Indian Institute of Technology Kharagpur, 721302, India

2 Centre for Ocean and Atmospheric Sciences, School of Environmental Sciences and School of Mathematics, University of East Anglia, Norwich, NR4 7TJ, United Kingdom

3 Climatic Research Unit, School of Environmental Sciences, University of East Anglia, Norwich, NR4 7TJ, United Kingdom

Corresponding author

Pranab Deb[1,3]

email: pranab@coral.iitkgp.ac.in, p.deb@uea.ac.uk

Abstract

Rossby wave trains triggered by tropical convection strongly affect the atmospheric circulation in the extratropics. Using daily gridded observational and reanalysis data, we demonstrate that a technique based on linear response theory effectively captures the linear response in 250-hPa geopotential height anomalies in the Northern Hemisphere, using examples of step-like changes in precipitation over selected tropical areas during boreal winter. Application of this method to six Coupled Model Intercomparison Project Phase 5 (CMIP5) models, using the same tropical forcing, reveals a large intermodel spread in the linear response, associated with intermodel differences in Rossby wave guide structure. The technique is then applied to a projected tropics-wide precipitation change in the HadGEM2-ES model during 2025-2045 DJF, a period corresponding to a 2°C rise in the mean global temperature under the RCP8.5 scenario. The response is found to depend on whether the mean state underlying the technique is calculated using observations, the present-day simulation, or the future projection; indeed, the bias in extratropical response to tropical precipitation because of errors in the basic state is much larger than the projected change in extratropical circulation itself. We therefore propose the linear step response method as a semi-empirical method of making near-term future projections of the extratropical circulation, which should assist in quantifying uncertainty in such projections.

Keywords: teleconnection, Rossby waves, CMIP5, model bias, tropical precipitation, Linear Response Theory, climate change, climate projections, constraint

1 Introduction:

Atmospheric tropical convection is a major driver of the global circulation. Through interaction with vorticity gradients in the subtropical jet streams, upper level divergence associated with anomalous tropical convection often leads to the formation of quasi-stationary Rossby waves in the extratropics (Hoskins and Karoly, 1981; Sardeshmukh and Hoskins, 1988; Matthews et al., 2004). Such teleconnection patterns influence several aspects of global climate and weather, e.g., the North Atlantic Oscillation (Lin et al., 2009), quasi-stationary blocking events (Henderson et al., 2016) cyclone frequency over the Northern Hemisphere (Eichler and Gottschalck, 2013), the South Asian monsoon (Shaman and Tziperman, 2005), and sea ice cover and ice shelf melting over coastal Antarctica (Deb et al., 2018; Liu et al., 2004).

The effect of tropical convective diabatic heating on the global circulation can be quantified dynamically by the Rossby wave source (e.g. Sardeshmukh and Hoskins, 1988; Scaife et al 2017), which takes account of both vortex stretching due to upper-tropospheric divergence, and advection of mean vorticity gradients by the anomalous flow associated with the divergence. Because the effective Rossby wave source depends on the structure and amplitude of the tropical heating anomaly (Hoskins and Karoly, 1981; Jin and Hoskins, 1995), any inherent model bias in the structure of tropical convection may lead to a bias in the generation and amplitude of extra-tropical Rossby waves (Henderson et al., 2017). Changes in the model basic state can also lead to differences in Rossby wave propagation, as subtle changes in the time-mean extratropical upper tropospheric zonal wind have a large dynamical effect on the Rossby wave propagation (Dawson et al., 2011). Similarly, Henderson et al. (2017) showed that errors in simulating Madden–Julian oscillation (MJO) teleconnections were due to the error in the model basic state, rather than in the MJO heating structure. Additionally, biases in Rossby wave propagation can themselves contribute to model biases in the representation of the extratropical mean circulation (Shepherd, 2014; Zappa et al., 2013). The biases in the model basic state extratropical jet structure can arise themselves from tropical-extratropical interactions, when biases in the tropical sea surface temperature field due to incorrectly modelled oceanic processes lead ultimately to biases in the extratropical jet structure (Dawson et al., 2013).

The global hydrological cycle, when measured by global precipitation, is generally expected to intensify under a warming climate in the future (Allen and Ingram, 2002). Despite the intermodel spread in CMIP5 models (Kent et al., 2015), both total precipitation and precipitation extremes over the tropics are expected to increase by the end of the twenty-first century (Kharin et al., 2013; Seager et al., 2010; Xie et al., 2010). Such projected changes in the tropical precipitation pattern are likely to modify present-day Rossby wave teleconnections, and induce changes in the extratropical circulation over the Northern Hemisphere. However, given large intermodel spreads in representations of the mean circulation in both present-day simulations and future projections, projected changes in teleconnections are very uncertain in the Northern Hemisphere.

The extratropical Rossby wave response in the upper troposphere triggered by anomalous tropical convection is mostly linear (Li et al., 2015), in that its amplitude scales with the amplitude of the forcing, but its structure remains mainly independent of the amplitude of the forcing. The Rossby wave response develops into a quasi-stationary pattern within about two weeks (Hoskins and Ambrizzi, 1993). Therefore, the quasi-stationary response that develops in the extratropics (e.g., geopotential height anomaly in the upper troposphere) may be expressed mathematically as a series of impulse responses convoluted with a previous history of tropical forcing. Such impulse responses can be represented by quasi-Green’s functions (Hasselmann et al., 1993). The tropical forcing can be usefully represented by precipitation anomalies, as precipitation anomalies are scaled versions of the convective diabatic heating anomalies, assuming the rain-out occurs in the same grid box as the condensation process that led to the diabatic heating. A ‘step’ response computed using these impulse response functions (G's) can therefore capture the linear response in the extratropics due to Rossby waves forced by the tropical precipitation anomaly.

The main objective of this paper is to quantify the linear response in extratropical circulation over the Northern Hemisphere during boreal winter due to observed anomalies in tropical precipitation using the 'Linear Response Theory' outlined above. The focus will be on the Northern Hemisphere during the winter season, particularly over the Pacific sector, as the combination of intense tropical convection over the warm pool in the Maritime Continent and western Pacific, and the anchoring of the Northern Hemisphere subtropical jet and associated mean vorticity gradients by the Tibetan Plateau and Asia–Pacific land–sea contrasts, lead to a particularly strong and robust teleconnection response here. The representation of this linear response in six commonly used CMIP5 models is then presented and discussed in the context of stationary Rossby wave theory using idealised precipitation anomalies. Finally, using tropical precipitation projections from one model (HadGEM2-ES), and basic states from both model and observations, we show how linear 'step' response theory can be employed to constrain future projections of extratropical circulation response to climate change.

The Linear Response Theory method put forward here can also be viewed as a complementary technique to the idealised barotropic and baroclinic model experiments that have been used to gain dynamical insights into the impact of tropical convection on the extratropical circulation. Typically, a barotropic (single level) or baroclinic (multi-level) atmospheric model is linearised about an observed basic state (time-mean flow) and forced in the tropics. The forcing mimics the effect of tropical convection. For a barotropic (vorticity equation) model with a single layer in the upper troposphere, this forcing takes the form of the upper level divergent outflow associated with the convection (Hoskins and Ambrizzi, 1993). For a baroclinic (primitive equation) model, a direct (convective) heating term is applied to the thermodynamic equation (Jin and Hoskins, 1995). The model is typically "dry", with no explicit moisture. The dynamical equations of the model are then run forward in time, to simulate the global response to the imposed tropical forcing. This approach can lead to profound dynamical insights into the nature of the tropical-extratropical interactions, especially when used in a hierarchy of models of increasing complexity.

However, this approach has its limitations. The basic state is often hydrodynamically unstable, especially in the case of baroclinic models. This affords only a narrow time window, in which the direct extratropical response has developed, but before the signal is swamped by unstable growing modes. The extratropical response can also be sensitive to any damping time scales imposed (Ting and Sardeshmukh, 1993). There are uncertainties in some of the assumptions in these idealised models, e.g., the vertical structure of the heating imposed in the baroclinic model (Matthews et al., 2004). Given the idealised nature of these experiments, there may be missing physical processes in their setup.

The linear response theory model approach put forward here takes an “end to end” approach. The interior atmospheric dynamics and physics that lead to an extratropical response to a tropical forcing are handled implicitly by a statistical method. Hence, the shortcomings of the barotropic and baroclinic model experiments described above are avoided. However, the disadvantage is that it is difficult to gain dynamical insight from this technique alone. Hence, we propose that the linear response theory model technique may be used as a complementary approach to the problem of tropical-extratropical interaction, alongside the idealised barotropic and baroclinic modelling techniques.

2 Data and Methodology:

Using Linear Response Theory, the extratropical circulation anomaly over the Northern Hemisphere can be decomposed into two parts: (1) a linear part dependent on the tropical precipitation anomaly;

(2) a residual part due to natural variability in the extratropics. The underlying assumptions of Linear Response Theory are: (1) the extratropical response to tropical forcing is linear; (2) the effect of local non-linear feedbacks on the tropical forcing is minimal.

Using Linear Response Theory, we can express the signal (*S*) at time *t* (days), as a weighted sum of the previous history of the forcing (*F*) during the last *T* days. Mathematically, we can write:

$$S(t) = \int_0^T G(\tau)F(t-\tau)d\tau + \varepsilon, \qquad (1)$$

where *F* is the forcing time series, τ is lag, *G* is the "Green's function" or weights to be found, and ε is the residual (due to non-linear effects and variability of *S* which is unconnected to the forcing). In this study, signal *S* is the daily geopotential height anomaly at 250 hPa (Z'_{250}) over the extratropics and forcing *F* is the precipitation anomaly over the tropics. Daily anomalies are computed by removing the annual cycle (defined here as the time-mean and first six annual harmonics).

In discretised form:

$$S(t) \approx \sum_{i=0}^{N} G(\tau_i)F(t-\tau_i)\Delta\tau + \varepsilon. \qquad (2)$$

where $\Delta\tau$ is the time interval of the data (1 day in this study), and the upper limit corresponds to $N\Delta\tau = T$.

Following Kostov et al. (2017), $G(\tau_i)$ (for i = 0, …., N) is estimated using a linear least-squares regression of the signal (Z'_{250}) against the lagged forcing (i.e., tropical precipitation anomaly). Using the impulse response *G*'s, we compute the 'step' response at lag $\tau_j = j\,\Delta\tau$, due to tropical forcing as follows:

$$S_{step}(\tau_j) \approx \sum_{i=0}^{j} G(\tau_i)\Delta\tau \qquad (3)$$

The step response represents the extratropical response (in Z'_{250}) due to a unit step-like change of tropical precipitation in a given forcing area. In our first example below (see Fig. 1), the step response at a time lag τ is the accumulated response in Z'_{250} in two regions of the North Pacific (Fig. 1, red and blue boxes) in τ days, caused by an anomalous precipitation event of unit magnitude over the tropical eastern Indian Ocean (Fig. 1 magenta box) which persists from lag 0 through to lag τ. The residual term ε denotes the remaining variability that cannot be explained by the tropical forcing. It contains the natural variability of the extratropics as well as uncertainty due to non-linear interactions. The results were not sensitive to the choice of level in the upper troposphere; calculations at 300 and 200 hPa led to a similar signal, as the extratropical response has an equivalent barotropic structure.

Daily geopotential height data are taken from the National Center for Environmental Prediction/National Center for Atmospheric Research (NCEP/NCAR) reanalysis (Kalnay et al., 1996) while the daily precipitation data are the 3B42 product from the Tropical Rainfall Measurement Mission (TRMM; Huffman et al., 2010). Since the quasi-stationary Rossby wave develops within about two weeks after the tropical forcing is switched on, computations up to a maximum time lag of T=40 days is sufficient to capture a fully developed Rossby wave response.

As a first example of the framework, the response is computed to a ‘forcing’ consisting of the daily precipitation anomaly, area averaged over the tropical eastern Indian Ocean (magenta box in Fig. 1). The response was calculated using Z'_{250} data from each day during the DJF seasons from 1998/99 to 2017/18. The forcing data were appropriately (negatively) lagged; therefore, for high negative lags, forcing data were used from the preceding October and November, as well as from the DJF season. The eastern Indian Ocean forms a part of the Indo-Pacific warm pool and is characterised by high sea surface temperatures and extensive, deep atmospheric convection. A typical upper tropospheric Rossby wave triggered by tropical forcing manifests as a spatial pattern of alternating positive and negative geopotential height anomaly centres in the extratropics. The propagation path is shown schematically by the thick yellow line in Fig. 1. The 'signal' is chosen as the daily geopotential height anomaly at 250 hPa (hereafter Z'_{250}) during DJF 1998/99-2017/18, averaged over a region in the extratropics. In this first example, the response is examined in two regions (shown by red and blue boxes in Fig. 1) which are chosen to capture the development of positive and negative Z'_{250} centres along the Rossby wave path.

To check that the forcing box does actually describe the forcing region, a correlation map between area-averaged precipitation over the forcing box against grid-point precipitation anomalies over the whole Northern Hemisphere is constructed. Significant correlations are found only over the forcing box (not shown), confirming that the forcing is restricted to the chosen box with no significant influences from other regions.

The linear step response in Z'_{250} to the precipitation anomaly over the eastern Indian Ocean is negative for the red box (Fig. 2a) and positive for the blue box (Fig. 2b). In both regions the response starts developing on the first day of the precipitation event and matures into a quasi-stationary value within a period of 15 - 20 days, which is consistent with our physical understanding of Rossby wave development. The average step response is obtained by averaging the quasi-stationary step responses over 30-40 day lags, and this 'average' step response can thus be used to represent the linear extratropical response due to tropical step-like precipitation changes. Note that the step response pattern was not sensitive to the exact choice of the 30-40 day lag window. The methodology is then extended to compute the averaged step response in Z'_{250} (averaged over 30 - 40 days) at each grid point over the Northern Hemisphere to capture the linear response over the entire Northern Hemisphere due to tropical forcing over a specific area.

The effects of the background atmospheric flow on the amplitude and propagation path of Rossby waves are demonstrated using the total stationary Rossby wavenumber (K_s) derived from the mean zonal wind field (Hoskins and Ambrizzi, 1993; Dawson et al., 2011), as follows:

$$K_s = \left(\frac{\beta - \bar{u}_{yy}}{\bar{u}}\right)^{1/2}, \qquad (4)$$

where $\bar{u}$ is the time-mean zonal wind, β is the meridional planetary vorticity gradient, and $\bar{u}_{yy}$ is the time-mean meridional relative vorticity gradient.

Rossby waves are refracted towards higher values of K_s and away from lower values of K_s such that regions with local maxima in K_s (e.g., mid-latitude westerly jets) act as waveguides for Rossby waves. This diagnostic has proved to be very useful in studying the Rossby wave propagation in the extra-tropics (Hoskins and Ambrizzi 1993; Ting and Sardeshmukh 1993; Dawson et al., 2011).

3 Extratropical linear response to tropical precipitation in present-day conditions

(a) Observations

The averaged linear step responses during DJF forced by tropical precipitation anomalies over the eastern Indian Ocean and the Maritime Continent are shown in Fig. 3a and 3b respectively. The linear response is scaled by the precipitation variability over the forcing region (which is approximately 3 mm day^{-1}). The linear response is significant over the northern Pacific Ocean with positive Z'_{250} centres over Eastern China and the central North Pacific Ocean, and a negative Z'_{250} centre over a region of East Asia/western Pacific Ocean covering Japan and the Korean Peninsula. Fig. 3b also suggests a significant negative-NAO type pattern over Western Europe associated with a positive rainfall anomaly over the Maritime continent.

The location and magnitude of the positive and negative anomaly centres are representative of canonical extra-tropical Rossby wave responses (approximately zonal wavenumber 4) in the Northern Hemisphere, as demonstrated in previous studies (Sardeshmukh and Hoskins, 1988; Matthews et al., 2004; Henderson et al., 2017). One interesting feature is the lack of sensitivity of the linear response over the northern Pacific Ocean to the actual location (longitude) of the tropical forcing. This is expected since the effective Rossby wave source is primarily dependent on the location of the westerly jet (Jin and Hoskins, 1995). This real-world linear extra-tropical response is now compared against linear responses from six selected global climate models.

(b) Climate models

Figure 4 shows the linear step response over 20 DJF seasons (scaled by 3 mm day^{-1}) in pre-industrial control integrations of six CMIP5 models (HadGEM2-ES, CCSM4, IPSL-cm5a-MR, GFDL-esm2G, MIROC5 and MPI-esm-MR), with the forcing location fixed over the eastern Indian Ocean (Fig. 4 magenta box). All six models show biases in the representation of the magnitude and spatial pattern of the linear step response when compared with Fig. 3a. Of the six models, HadGEM2-ES and MPI-esm-MR show comparatively better skill in capturing the positive and negative anomaly centres over the northern Pacific Ocean (Fig. 4a and 4f). However, the spatial structure of the positive anomaly centres over the northern Pacific Ocean is better represented by MPI-esm-MR compared to HadGEM2-ES. Such subtle differences are very important for regional weather over North America and East Asia. These two models also correctly simulate the positive and negative anomaly centres over the western coast of USA (Baja California) and the north-western coast of Canada, respectively. The performances of these two models deteriorate away from the North Pacific Ocean.

The remaining four models show large errors over the whole Northern Hemisphere with CCSM4 and MIROC5 simulating an annular response over the North Pacific Ocean (Fig. 4b and 4e). Interestingly, all the GCMs display significant responses over the Atlantic/European region; indeed the significance of the responses appear to be greater than the observed response (Fig. 3a). The patterns of the GCM responses are however all different. Such differences are commented on below.

Similarly, Fig. 5 shows the linear step response (scaled by 3 mm day^{-1}) in the same six CMIP5 models with the forcing location fixed over the Maritime Continent. All the models show significant biases in the representation of the linear extratropical response. HadGEM2-ES captures the positive anomaly centre over East Asia well and only partially captures the negative anomaly centre over Japan/Korean peninsula, but fails to reproduce the linear response over the rest of the domain. The spatial pattern of linear response for HadGEM2-ES resembles that for IPSL-cm5-MR over the Pacific Ocean. For the remaining models, e.g., GFDL-esm2G, MIROC5 and MPI-esm-MR, the linear response is similar to a Pacific North American (PNA) teleconnection pattern rather than a typical Rossby wave response forced by convection over the Maritime Continent.

(c) Rossby wave guides

An advantage of the Linear Response Theory is that it allows us to study the extratropical response in each of the CMIP5 models due to identical persistent observed precipitation anomalies over a specific region. Hence, the differences in linear response are due directly to the incorrect representation of the teleconnection itself, not to the erroneous representation of precipitation in the models. To understand the role of the atmospheric basic state, the total stationary wavenumber (K_s) is computed from the mean zonal wind at 250 hPa of the six CMIP5 models (Fig. 6a-f), and is compared against reanalysis data (Fig. 6g).

Linear Rossby waves cannot propagate through areas with easterly winds (black shading) or areas with negative β^* (where $\beta^* = \beta - \bar{u}_{yy}$, shown in grey shading), which are often found on the poleward side of the subtropical jet. Together with the waveguide nature of the jet itself, this implies that Rossby waves can propagate poleward only after exiting the subtropical jet. When the jet is extended eastward, the area of negative β^* also tends to extend eastward, which is associated with a more zonally-extended structure of the waveguide (Fig. 6c, & 6e). Thus, biases in the structure and zonal extent of the jet lead to changes in the Rossby wave guide and the subsequent propagation paths of Rossby waves. In Fig. 6, zonal wavenumbers 4 and 5 have been highlighted (white contours) to show the Rossby waveguide for a typical planetary-scale Rossby wave.

Some of the CMIP5 models, with more zonally extended regions of negative β^* (grey area in Fig. 6c & 6e) compared to reanalysis (Fig. 6g), have a more extended zonal waveguide compared to reanalysis. In contrast, models with a more realistic jet structure have a northeastward extension of the Rossby waveguide reaching up to North America (Fig. 6a & 6f) which agrees well with reanalysis (Fig. 6g). Despite a realistic structure of the negative β^* area, the end of the Asia-Pacific waveguide is not properly represented in CCSM4 (Fig. 6b).

Over North America, the signature of two Rossby waveguides can be seen in reanalysis data (Fig. 6g): the end of the subtropical Asia-Pacific jet waveguide (~ 50 °N) and the beginning of Atlantic-African jet waveguide (~ 20 °N). These two waveguides are separated by an area of low zonal wavenumber which will oppose Rossby wave propagation between them. Most of the CMIP5 models, except HadGEM2-ES, do not have this clear separation between the waveguides. Hence in these models, due to the close proximity of the two waveguides, Rossby waves are expected to be refracted towards the tropical waveguide on reaching the end of the Asia-Pacific jet stream. This subtle dynamical bias in the models may result in significant errors in the extra-tropical Rossby wave response. In contrast, HadGEM2-ES shows a well-defined structure for both the waveguides (Fig. 6a), with a small area of negative β^* separating them (grey shading). Thus, overall, a more realistic representation of the basic atmospheric state and hence the Rossby waveguide structure in HadGEM2-ES (Fig. 6a) allows a comparatively better representation of the extra-tropical Rossby wave response (e.g., Fig. 4a), than in the other models.

(d) Extratropical response during El Niño events

Before applying the linear response technique to the problem of climate change, we test it by evaluating its effectiveness in capturing the well-known extratropical response to El Niño. To this end, a similarity projection metric $\sigma(t_j)$ at each time t_j is first computed. This is defined as the inner product (defined as the sum of the element-wise product of two matrices) between the map of a composite El Niño precipitation anomaly x (DJF mean of five recent El Niño years: 2002/03, 2004/05, 2006/07, 2009/10 and 2015/16) and daily maps of precipitation anomalies $\boldsymbol{y}(t_j)$ from TRMM (DJF, 1998/99-2017/18), over the tropical belt 20°S – 20°N:

$$\sigma(t_j) = x \,.\, y(t_j) \qquad (5)$$

Thus, the similarity projection metric is a daily time series, with a value for each day in DJF from 1998/99 to 2017/18. Higher values of the metric correspond to higher similarity (in both magnitude and pattern) between the map of the composite El Niño precipitation anomaly and the map of the daily precipitation anomaly.

By using this similarity projection metric as the forcing time series (F) in eqn. (2), we can assess the performance of the step response method in simulating the actual extra-tropical response during El Niño periods. The step response to the El Niño precipitation forcing (Fig. 7a) shows strong similarity to the composite Z'_{250} map for selected El Niño years (DJF, 2002/03, 2004/05, 2006/07, 2009/10, 2015/16) (Fig. 7b). The step response in fig. 7a closely resembles the canonical El Niño teleconnection pattern characterised by a robust PNA pattern (Diaz et al., 2001; Straus and Shukla, 2002; Toniazzo and Scaife, 2006). This suggests that the response to El Niño Southern oscillation (ENSO) can be well approximated by this methodology, suggesting that under a moderate warming scenario (e.g., 2 °C rise in global mean temperature), where the jet stream is not expected to change significantly, the Linear Response Theory may be applied to provide a prediction of near-term changes in extratropical circulation.

4 Extratropical linear response due to future changes in tropical precipitation

a. Similarity projection metric of future precipitation change

The large intermodel spread in linear step response function over the North Pacific arises due to the variability in the spatial extent and strength of the Pacific jet stream among the CMIP5 models. In a warming world, Arctic amplification is generally expected to reduce the low-level meridional (equator-pole) temperature gradient. Conversely, the upper-tropospheric equator–pole temperature gradient will increase because of changes in moist adiabatic lapse rate predominantly in the tropics (Vallis et al. 2015) and greenhouse gas-induced cooling in the polar lower stratosphere. Because of the uncertainty in the future changes in tropospheric temperature gradient, the future projection of Northern Hemisphere circulation and the mid latitude jet stream remains uncertain (Harvey et al., 2014; Barnes and Screen, 2015). It is therefore expected that uncertainties in CMIP5 projections of extratropical Rossby wave response will also increase into the future.

We now consider an alternative approach to projecting future changes in the extratropical mean state: calculating the linear step response function from projected precipitation anomalies, using observed representations of Z'_{250}. Using the linear step response function computed for the observed basic state avoids the sizeable step response biases that occur when using the basic states of climate models (Section 3). The linear step response method is therefore another approach to making projections of extratropical circulation compared to using the CMIP5 models themselves.

Here, we employ this methodology to assess changes between the present day and DJF 2025-2045, which corresponds to an approximate 2°C rise in global mean temperature from the pre-industrial era under a high emission scenario (RCP 8.5) in HadGEM2-ES. The choice of a near-term projection is made in order to reduce changes in the atmospheric basic state expected from the large increase in global mean temperature towards the end of the 21st century in HadGEM2-ES. In addition, a large uncertainty exists in the future projection of the magnitude and spatial pattern of tropical precipitation change itself in the later part of the 21st century (Oueslati et al., 2016; Knutti et al., 2013), although much of this is because of differences in the projected changes in global mean temperature (Knutti et al., 2016). Therefore, choosing the future period based on a 2°C rise should also help minimise the intermodel spread in future projection of tropical precipitation.

To assess the extratropical response due to future tropical precipitation changes, a similarity projection metric is first computed in a similar manner to that for El Niño in Section 3d (Eq. 5). First, an anomaly map x is created from the difference between the map of future (DJF, 2025/26-2045/46) and the present day precipitation (DJF, 1986/87-2005/06) from the model. For HadGEM2-ES this difference map shows increases in precipitation over the Maritime Continent, western Pacific Ocean and eastern Indian Ocean, decreases over the western Indian Ocean and an equatorward (southward) shift of the Intertropical Convergence Zone over the central and eastern Pacific (Fig. 8d). As in Section 3d, a similarly projection metric $\sigma(t_j)$ is then calculated as the inner product between this anomaly map x and daily maps of precipitation anomalies from modern day observations of precipitation $y(t_j)$ (TRMM: DJF, 1998/99-2017/18), over the tropical belt 20°S – 20°N. Again this produces a time series with daily values of the similarity projection metric from 1998/99-2017/18. In this case, higher values of the metric correspond to higher similarity (in both magnitude and pattern) between the map of future precipitation change and the map of the daily precipitation anomaly.

A composite map of TRMM precipitation anomalies corresponding to the days when the similarity projection metric values are in their upper quartile (Fig. 8a) shows close agreement with the projected precipitation change (Fig. 8d), confirming the validity of this technique. Thus using the similarity projection metric as forcing (F) in Eq. 2, we are effectively forcing the present-day extra-tropical circulation with the projected future precipitation change. This addresses the question – what will be the linear extra-tropical response within the present climate state, if forced by a tropical precipitation anomaly similar to future precipitation change?

b. Step response function to future precipitation change on present observed basic state

Figure 9a shows the step response function (averaged over lag 30-40 days) computed using Z'_{250} from NCEP/NCAR reanalysis (DJF, 1998/99-2017/18) as the signal, and forced by one standard deviation of this similarity projection metric. This can be physically interpreted as the linear extratropical step response if the future simulated tropical precipitation change occurred in the present-day observed climatic state. A strong extratropical response emerges over the entire Northern Hemisphere. The extratropical response in Z'_{250} is characterised by a clear Rossby wave pattern over the northern Pacific Ocean with positive Z'_{250} centres over eastern China and the central North Pacific Ocean, and a negative Z'_{250} centre over a region of northeast Asia/western Pacific Ocean. Additionally, a negative Z'_{250} centre appears over the Mediterranean Sea/North Africa region while a positive Z'_{250} centre develops over the North Atlantic Ocean. Overall, the spatial pattern of Z'_{250} in Fig. 9a is very roughly equivalent to a superposition of the step responses in Fig. 3a and 3b. This is because the strongest increases in future precipitation (during DJF 2025-2045) are centred over the eastern Indian Ocean and the Maritime Continent (i.e., the forcing regions in Fig. 3) which underlines the linear nature of extratropical response due to tropical forcing (precipitation).

c. Step response function to future precipitation change on present model basic state

Figure 9b shows the average step response function computed using Z'_{250} from the present HadGEM2-ES simulation (DJF, 1986/87-2005/06), and forced by one standard deviation of a different similarity projection metric, calculated as the inner product of the maps of the same future tropical precipitation change x, and daily HadGEM2-ES model precipitation anomalies $\boldsymbol{y}(t_j)$ during the 1986-2005 period. A map of this forcing (Fig. 8b) is very similar to the forcing in Fig. 8a. In other words, Fig. 9b represents the linear extratropical step response if the future tropical precipitation change (as simulated by HadGEM2-ES) occurred in the present model climatic state. The extratropical response in Fig. 9b is characterised by weak negative Z'_{250} centres over north-eastern Russia and Alaska, and a positive Z'_{250} centre over North Atlantic Ocean. It is evident that there are large differences between Figs. 9a and 9b in terms of both the magnitude and spatial extent of extratropical response due to future changes in tropical precipitation.

d. Step response function to future precipitation change on future model basic state

The simulated extratropical linear response due to future tropical precipitation change under the future model climatic state (here $\boldsymbol{y}(t_j)$ are the daily HadGEM2-ES precipitation anomalies during the *2025/26-2045/46 period*) is shown in Fig. 9c. Again, the forcing (Fig. 8c) is very similar to the forcing in Fig. 8a, and the difference in extratropical response can be interpreted as being solely due to changes in the basic state. Only a weak extratropical response can be seen over the northern Pacific Ocean while a positive Z'_{250} centre appears over Scandinavia. Overall, the future dynamical change in the extratropical linear response (comparison of Fig. 9c and 9b) appears to be much smaller than the bias in the model's linear response within the present climate state (comparison of Fig. 9a against 9b).

e. Actual projected change in extratropical circulation

Figure 9d shows the actual projected changes in average winter (DJF) geopotential height at 250 hPa (Z_{250}) during the future period 2025-2045 (relative to present/historical period 1986-2005) from the high emission scenario (RCP 8.5), as simulated by the HadGEM2-ES model. The strengthening of the meridional gradient in the Z_{250} change over south East Asia/China and the central Pacific Ocean (across the 30°N latitude) suggests a strengthening of both the East Asia jet stream and the Pacific subtropical jet stream in the future. There are differences in the extratropical response between the linear response theory predicated on either observations or model, and the model projection itself, which we comment on below.

5 Discussion and Conclusions

We have exploited the linear nature of the extratropical Rossby wave response to tropical forcing to demonstrate that such response (over the Northern Hemisphere) can be realistically quantified using Linear Response Theory. Initially, the forcing (i.e., tropical precipitation anomaly) is limited to a specific area of interest and the magnitude scaled to a standard value (i.e., 3 mm day^{-1}). Hence, despite the large intermodel spread in the spatial extent and magnitude of tropical precipitation, the extratropical signal is forced by the same magnitude of forcing in the six selected CMIP5 models.

The linear step response function derived using this approach is used to compare the extratropical teleconnection in selected CMIP5 models. The model performances vary widely with most of the models differing in the spatial extent and magnitude of the linear response, because of differences in their mean states, encapsulated by the Rossby waveguide. In the observations, as represented by the reanalysis data, an area of negative (reversed) absolute vorticity gradient (β^*), often found on the poleward side of the Northern Hemisphere subtropical jet, restricts the Rossby waves to the south. On exiting the jet stream, the Rossby waveguide (highlighted by zonal stationary wavenumbers 4-5) shows a northeastward extension to North America. With a notable exception, this feature is not generally well represented by the CMIP5 models.

The Linear Response Theory method (LRTM) is employed to analyse the DJF extratropical response to El Niño events, and performs well, simulating the observed PNA response. There are differences in response between the LRTM and observations over the Euro-Atlantic region, where the former simulates a positive NAO-like pattern. However, the Atlantic response to El Niño events is significantly affected by non-linear changes to the stratospheric circulation during such times (e.g. Bell et al. 2009), which are not represented in the LRTM. Despite this, the performance of the LRTM does suggest some potential role for seasonal prediction, as a semi-empirical prediction with which CMIP models can be compared. Suggested future work in this direction could involve comparing interannual variability in the extratropical state using the LRTM and CMIP model hindcasts, particularly in the European-Atlantic region. Such work would examine how well the LRTM, with its lack of mean-state biases but also caveats, performs against CMIP models that predict many, but by no means all, aspects of interannual variability in this region (e.g., Eade et al. 2014).

The LRTM is then compared against a standard projection of extratropical circulation in HadGEM2-ES when global temperature change reaches 2°C. The model is chosen because it represents well the separation between the subtropical Asia-Pacific jet waveguide (~ 50°N) and the Atlantic-African jet waveguide (~ 20°N) (by an area of low zonal wavenumber), which opposes Rossby wave propagation. There are notable differences between the LRTM extratropical response using simulated precipitation changes and observed present-day state (Fig. 9a), simulated precipitation changes and simulated present-day state (Fig. 9b), and the CMIP model itself (Fig. 9d). Given the good performance of the LRTM in simulating the extratropical response to El Niño, one cannot assume that the direct GCM projection of extratropical circulation change (Fig. 9d) is automatically “better” than the equivalent projection made using the LRTM (Fig. 9a). Quantifying the skill of the LRTM vs CMIP projections is the next step, and accordingly future work will utilise sets of so-called “perfect model” experiments in order to quantify to what extent the LRTM can be used in tandem with standard CMIP model projections to quantify uncertainty in the extratropical circulation response to climate change.

We note again that the use of the LRTM for making future projections is contingent on small changes in the mean extratropical state, so that changes in the mean state in the future are small compared to biases in simulated mean model states. The LRTM is therefore not suitable for projecting change under large degrees of warming (or indeed cooling). The LRTM is dependent on using projected tropical model precipitation changes, and so can, at best, only reduce that level of bias which arises from CMIP model representations of the extratropical mean state. If GCMs have common biases in tropical precipitation projections, which recent work suggests is possible (Seager et al. 2019), such common biases will feed through into projections made using the step response method as well.

Our study highlights the use of the linear step response function (computed using a LRTM) as a new method for calculating Northern Hemisphere extratropical circulation responses to tropical precipitation anomalies. The utility of the method lies in its use of observations of the Northern Hemisphere extratropical mean state, thus eliminating biases in its representation from degrading model response. The method does have drawbacks, such as its assumption of linearity, and hence its inability to simulate the extratropical response to tropical precipitation anomalies via non-linear stratospheric and tropospheric processes, but represents the extratropical response to El Niño events well. We hope to compare this method in future with standard near-term projections made using CMIP models, in order to assist in quantifying uncertainty in future extratropical changes.

Acknowledgements:

We thank the World Climate Research Programme and the different modelling groups for producing and sharing the CMIP5 model output. The TRMM 3B42 data were downloaded from NASA-Goddard, and ERA-Interim Reanalysis data were downloaded from the Centre for Environmental Data Analysis. PD was supported by UK NERC grant NE/N018486/1 Robust Spatial Projections Of Real-World Climate Change. We sincerely thank the anonymous reviewers whose comments helped improve the readability of our manuscript.

References:

Allen, M. R., and W. J. Ingram, 2002: Constraints on future changes in climate and the hydrologic cycle. *Nature,* **419**, 224–232, doi: 10.1038/nature01092.

Barnes, E. A., and J. A. Screen, 2015: The impact of Arctic warming on the midlatitude jetstream: Can it? Has it? Will it? *WIRES Climate Change,* **6,** 277–286, doi: 10.1002/wcc.337.

Bell, C. J., L. J. Gray, A. J. Charlton-Perez, M. M. Joshi and A. A. Scaife, 2009: Stratospheric Communication of El Niño Teleconnections to European Winter, *J. Climate,* **22,** 4083-4096, doi: 10.1175/2009JCLI2717.1.

Bernstein L, Bosch P, Canziani O, Chen Z, Christ R, and Riahi K, 2008: IPCC, 2007: Climate Change 2007: Synthesis Report. Geneva: IPCC. ISBN 2-9169-122-4.

Dawson, A., A.J. Matthews, and D.P. Stevens, 2011: Rossby wave dynamics of the North Pacific extra-tropical response to El Niño: importance of the basic state in coupled GCMs. *Clim Dyn*, **37**, 391, doi: 10.1007/s00382-010-0854-7.

Dawson, A., A. J. Matthews, D. P. Stevens, M. J. Roberts, and P. L. Vidale, 2013: Importance of oceanic resolution and mean state on the extra-tropical response to El Nino in a matrix of coupled models. *Climate Dyn.,* **41,** 1439-1452, doi: 10.1007/s00382-012-1518-6.

Deb, P., A. Orr, D. H. Bromwich, J. P. Nicolas, J. Turner, and J. S. Hosking, 2018: Summer drivers of atmospheric variability affecting ice shelf thinning in the Amundsen Sea Embayment, West Antarctica. *Geophysical Research Letters*, **45**, 4124– 4133, doi: 10.1029/2018GL077092.

Diaz, H. F., M. P. Hoerling, and J. K. Eischeid, 2001: ENSO variability, teleconnections and climate change. *Int. J. Climatol.*, **21**, 1845-1862, doi:10.1002/joc.631.

Eade, R., D. Smith, A. Scaife, E. Wallace, N. Dunstone, L. Hermanson, N. Robinson, 2014: Do seasonal-to-decadal climate predictions underestimate the predictability of the real world? *Geophys. Res. Lett.*, **41**, 5620–5628, doi: 10.1002/2014GL061146.

Eichler T. P., and J. Gottschalck, 2013: Interannual Variability of Northern Hemisphere Storm Tracks in Coarse-Gridded Datasets. *Advances in Meteorology*, vol. **2013**, Article ID 545463, 15 pages, doi: 10.1155/2013/545463.

Harvey, B.J., L.C. Shaffrey, and T.J. Woollings, 2014: Equator-to-pole temperature differences and the extra-tropical storm track responses of the CMIP5 climate models. *Clim Dyn*, **43**: 1171-1182, doi: 10.1007/s00382-013-1883-9.

Hasselmann, K, R Sausen, E Maier-Reimer, and R Voss, 1993: On the cold start problem in transient simulations with coupled atmosphere-ocean models. *Climate Dynamics*, **9**, 53-61, doi: 10.1007/BF00210008.

Henderson, S. A., E. D. Maloney, and E. A. Barnes, 2016: The influence of the Madden-Julian oscillation on Northern Hemisphere winter blocking. *Journal of Climate*, **29**, 4597– 4616, doi: 10.1175/JCLI-D-15-0502.1.

Henderson, S.A., E.D. Maloney, and S. Son, 2017: Madden–Julian Oscillation Pacific Teleconnections: The Impact of the Basic State and MJO Representation in General Circulation Models. *J. Climate*, **30**, 4567–4587, doi: 10.1175/JCLI-D-16-0789.1.

Hoskins, B. J., and D. J. Karoly, 1981: The steady linear response of a spherical atmosphere to thermal orographic forcing. *Journal of the Atmospheric Sciences*, **38**, 1179–1196, doi: 10.1175/1520-0469(1981)038<1179:TSLROA>2.0.CO;2.

Hoskins, B.J., and T. Ambrizzi, 1993: Rossby Wave Propagation on a Realistic Longitudinally Varying Flow. *J. Atmos. Sci.*, **50**, 1661–1671, doi: 10.1175/1520-0469(1993)050<1661:RWPOAR>2.0.CO;2.

Huffman, G.J., R.F. Adler, D.T. Bolvin, and E.J. Nelkin, 2010: The TRMM Multi-satellite Precipitation Analysis (TMPA). Chapter 1 in Satellite Rainfall Applications for Surface Hydrology, F. Hossain and M. Gebremichael, Eds. Springer Verlag, ISBN: 978-90-481-2914-0, 3-22.

IPCC, 2012: Summary for policymakers. Managing the Risks of Extreme Events and Disasters to Advance Climate Change Adaptation, C. B. Field et al., Eds., Cambridge University Press, 1–19.

Jin, F., and B.J. Hoskins, 1995: The Direct Response to Tropical Heating in a Baroclinic Atmosphere. *J. Atmos. Sci.*, **52**, 307–319, doi: 10.1175/1520-0469(1995)052<0307:TDRTTH>2.0.CO;2.

Kalnay and Coauthors, 1996: The NCEP/NCAR 40-year reanalysis project. *Bull. Amer. Meteor. Soc.*, **77**, 437-470, doi: 10.1175/1520-0477(1996)077<0437:TNYRP>2.0.CO;2.

Kent, C., R. Chadwick, and D.P. Rowell, 2015: Understanding Uncertainties in Future Projections of Seasonal Tropical Precipitation. *J. Climate*, **28**, 4390–4413, doi: 10.1175/JCLI-D-14-00613.1.

Kharin, V.V., F.W. Zwiers, and X. Zhang, 2013: Changes in temperature and precipitation extremes in the CMIP5 ensemble. *Climatic Change*, **119**, 345-357, doi: 10.1007/s10584-013-0705-8.

Knutti, R., and J. Sedláček, 2013: Robustness and uncertainties in the new CMIP5 climate model projections. *Nature Climate Change*, **3**, 369–373, doi: 10.1038/nclimate1716.

Knutti, R., J. Rogelj, J. Sedláček, and E. M. Fischer, 2016: A scientific critique of the two-degree climate change target. *Nature Geoscience*, **9**, 13–18. doi: 10.1038/ngeo2595.

Kostov, Y., J. Marshall, U. Hausmann, K. C. Armour, D. Ferreira, and M. M. Holland, 2017: Fast and slow responses of Southern Ocean sea surface temperature to SAM in coupled climate models. *Climate Dynamics*, **48**, 1595-1609, doi: 10.1007/s00382-016-3162-z.

Lee, M., S. Lee, H. Song, and C. Ho, 2017: The Recent Increase in the Occurrence of a Boreal Summer Teleconnection and Its Relationship with Temperature Extremes. *J. Climate*, **30**, 7493–7504, doi: 10.1175/JCLI-D-16-0094.1.

Li, X., E.P. Gerber, D.M. Holland, and C. Yoo, 2015: A Rossby Wave Bridge from the Tropical Atlantic to West Antarctica. *J. Climate*, **28**, 2256–2273, doi: 10.1175/JCLI-D-14-00450.1.

Lin, H., G. Brunet, and J. Derome, 2009: An observed connection between the North Atlantic Oscillation and the Madden-Julian Oscillation. *Journal of Climate*, **22**, 364–380, doi: 10.1175/2008JCLI2515.1.

Liu, J.P., X.J. Yuan, D.G. Martinson, and D. Rind, 2004: Re-evaluating Antarctic sea-ice variability and its teleconnections in a GISS global climate model with improved sea ice and ocean processes. *Int. J. Climatol.*, **24**, 841-852, doi:10.1002/joc.1040.

Matthews, A. J., B. J. Hoskins, and M. Masutani, 2004: The global response to tropical heating in the Madden-Julian Oscillation during Northern winter. *Quarterly Journal of the Royal Meteorological Society*, **130**, 1991– 2011, doi: 10.1256/qj.02.123.

Oliver, E. C. J., 2015: Multidecadal variations in the modulation of Alaska wintertime air temperature by the Madden–Julian Oscillation. *Theor. Appl. Climatol.*, **121**, 1–11, doi: 10.1007/s00704-014-1215-y.

Oueslati, B., S. Bony, C. Risi, and Jean-Louis Dufresne, 2016: Interpreting the inter-model spread in regional precipitation projections in the tropics: role of surface evaporation and cloud radiative effects. *Climate Dynamics*, **47**, 2801–2815. doi: 10.1007/s00382-016-2998-6.

Rahmstorf, S., and D. Coumou, 2011: Increase of extreme events in a warming world. *Proc. Natl. Acad. Sci. USA*, **108**, 17 905–17 909, doi: 10.1073/pnas.1101766108.

Sardeshmukh, P., and B. J. Hoskins, 1988: The generation of global rotational flow by steady idealized tropical divergence. *Journal of the Atmospheric Sciences*, **45**, 1228– 1251, doi: 10.1175/1520-0469(1988)045<1228:TGOGRF>2.0.CO;2.

Scaife, A. A., R. E. Comer, N. J. Dunstone, J. R. Knight, D. M. Smith, C. MacLachlan, N. Martin, K. A. Peterson, D. Rowlands, E. B. Carroll, S. Belcher and J. Slingo, 2017: Tropical rainfall, Rossby waves and regional winter climate predictions, *Q. J. R. Meteorol. Soc.*, **143**, 1-11, doi: 10.1002/qj.2910.

Seager, R., N. Naik, and G.A. Vecchi, 2010: Thermodynamic and Dynamic Mechanisms for Large-Scale Changes in the Hydrological Cycle in Response to Global Warming. *J. Climate*, **23**, 4651–4668, doi: 10.1175/2010JCLI3655.1.

Seager, R., M. Cane, N. Henderson, D.-E. Lee, R. Abernathey and H. Zhang, 2019: Strengthening tropical Pacific zonal sea surface temperature gradient consistent with rising greenhouse gases. *Nature Climate Change*, **9**, 517–522, doi: 10.1038/s41558-019-0505-x.

Seneviratne, S. I., M. G. Donat, B. Mueller, and L. V. Alexander, 2014: No pause in the increase of hot temperature extremes. *Nat. Climate Change*, **4**, 161–163, doi: 10.1038/nclimate2145.

Seo, K., H. Lee, and D.M. Frierson, 2016: Unraveling the Teleconnection Mechanisms that Induce Wintertime Temperature Anomalies over the Northern Hemisphere Continents in Response to the MJO. *J. Atmos. Sci.,* **73**, 3557–3571, doi: 10.1175/JAS-D-16-0036.1.

Shaman, J., and E. Tziperman, 2005: The Effect of ENSO on Tibetan Plateau Snow Depth: A Stationary Wave Teleconnection Mechanism and Implications for the South Asian Monsoons. *J. Climate*, **18**, 2067–2079, doi: 10.1175/JCLI3391.1.

Shepherd, T. G., 2014: Atmospheric circulation as a source of uncertainty in climate change projections. *Nature Geoscience*, **7,** 703– 708, doi: 10.1038/ngeo2253.

Straus, D.M., and J. Shukla, 2002: Does ENSO Force the PNA?. *J. Climate*, **15**, 2340–2358, doi: 10.1175/1520-0442(2002)015<2340:DEFTP>2.0.CO;2.

Ting, M., and P.D. Sardeshmukh, 1993: Factors Determining the Extratropical Response to Equatorial Diabatic Heating Anomalies. *J. Atmos. Sci.*, **50**, 907–918, doi: 10.1175/1520-0469(1993)050<0907:FDTERT>2.0.CO;2.

Toniazzo, T., and Scaife, A. A. (2006), The influence of ENSO on winter North Atlantic climate, *Geophys. Res. Lett.*, **33**, L24704, doi:10.1029/2006GL027881.

Vallis, G. K., P. Zurita-Gotor, C. Cairns, and J. Kidston, 2015: Response of the large-scale structure of the atmosphere to global warming. *Quart. J. Roy. Meteor. Soc.*, **141**, 1479–1501, doi: 10.1002/qj.2456.

Xie, S., C. Deser, G.A. Vecchi, J. Ma, H. Teng, and A.T. Wittenberg, 2010: Global Warming Pattern Formation: Sea Surface Temperature and Rainfall. *J. Climate*, **23**, 966–986, doi: 10.1175/2009JCLI3329.1.

Zappa, G., F. Pithan, and T. G. Shepherd, 2018: Multimodel evidence for an atmospheric circulation response to Arctic sea ice loss in the CMIP5 future projections. *Geophysical Research Letters*, **45**, 1011– 1019, doi: 10.1002/2017GL076096.

Zhan, R., Y. Wang, and L. Tao, 2014: Intensified Impact of East Indian Ocean SST Anomaly on Tropical Cyclone Genesis Frequency over the Western North Pacific. *J. Climate*, **27**, 8724–8739, doi: 10.1175/JCLI-D-14-00119.1.

Figure 1: Schematic diagram of the tropical-extratropical interaction mechanism underlying the linear response theory. A tropical precipitation anomaly (in this example in the eastern Indian Ocean; magenta box, 80-110 °E, 15 °S-15 °N) triggers an extratropical Rossby wave response (path shown by yellow arrow). This interacts with the subtropical jet stream (orange arrows), and leads to a region of negative 250-hPa geopotential height anomaly over the western north Pacific (red box, 125-155 °E, 30-45 °N) and an area of positive 250-hPa geopotential height anomaly over the central north Pacific (blue box, 180-210 °E, 30-45 °N).

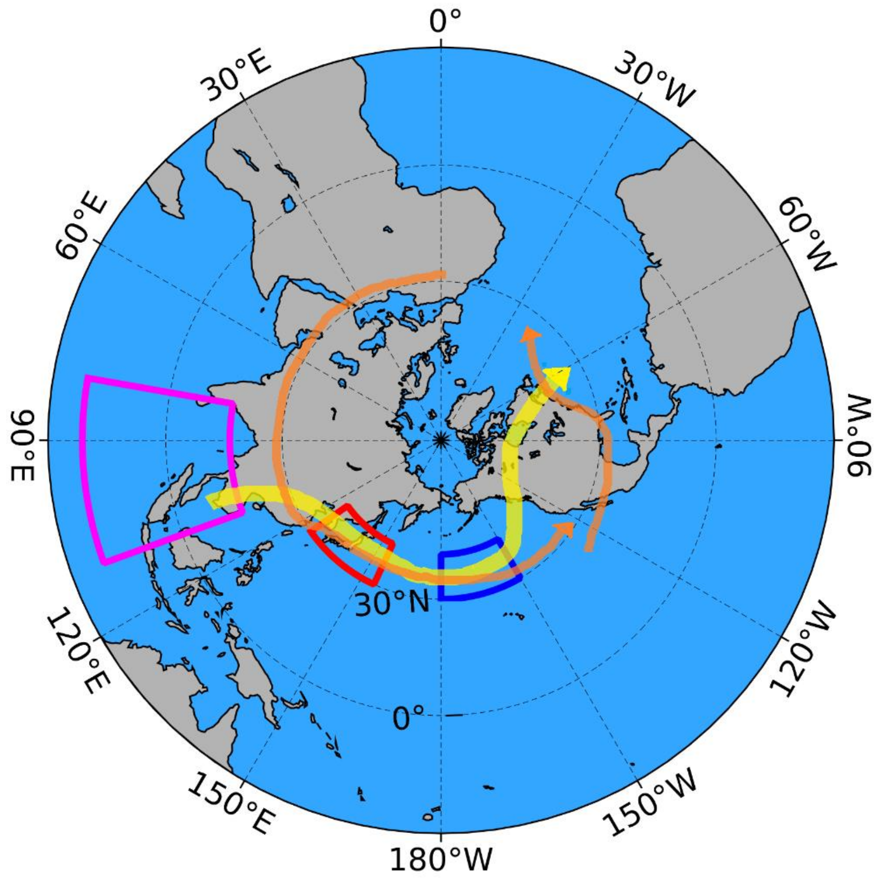

Figure 2: Step response function for anomalous 250-hPa geopotential height (NCEP/NCAR reanalysis) over the North Pacific, averaged over (a) 125-155 °E, 30-45 °N (shown by red box in Fig. 1), (b) 180-210 °E, 30-45 °N (shown by blue box in Fig. 1), forced by a 3 mm day^{-1} precipitation (TRMM) anomaly over the eastern Indian Ocean (averaged over 80-110 °E, 15 °S-15 °N, magenta box in Fig. 1), during DJF, 1998/99-2017/18.

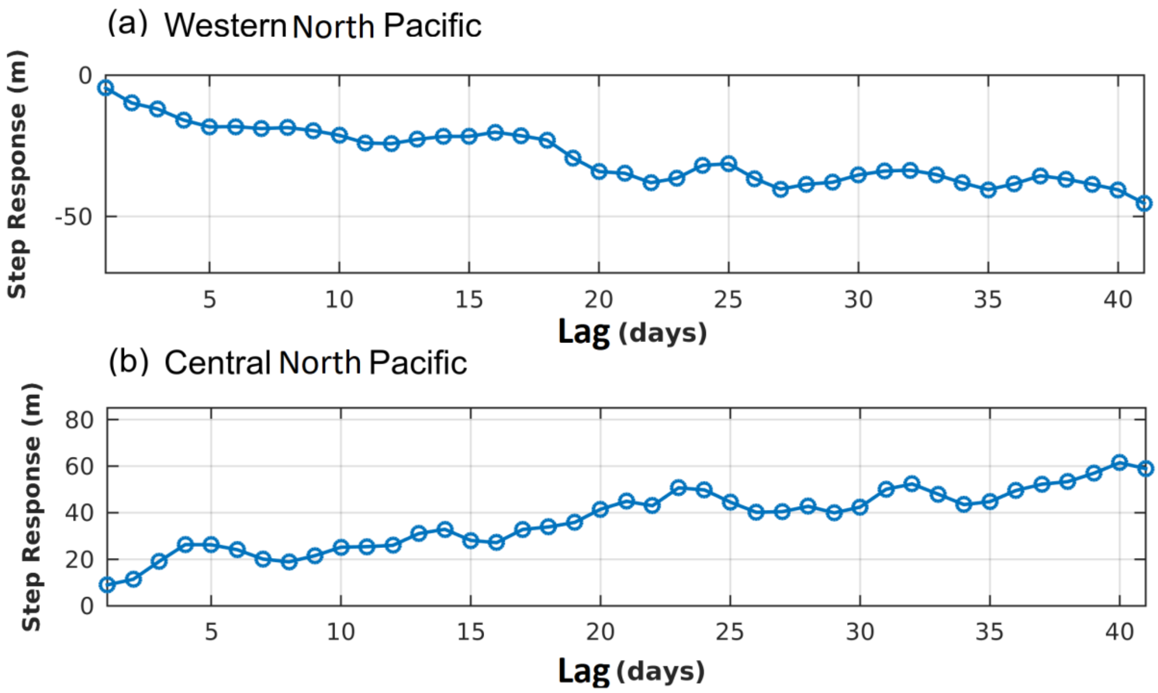

Figure 3: Step response function for anomalous 250-hPa geopotential height (NCEP/NCAR reanalysis), averaged over lag 30-40 days, forced by 3 mm day^{-1} area-averaged precipitation (TRMM) anomaly over the (a) eastern Indian Ocean, and (b) Maritime Continent (shown by the magenta boxes), during DJF, 1998/99-2017/18. Shading and contour interval is 10 m. Shading is masked out where the step response function is less than one standard deviation, and contour lines are only plotted where the step response function is more than two standard deviations.

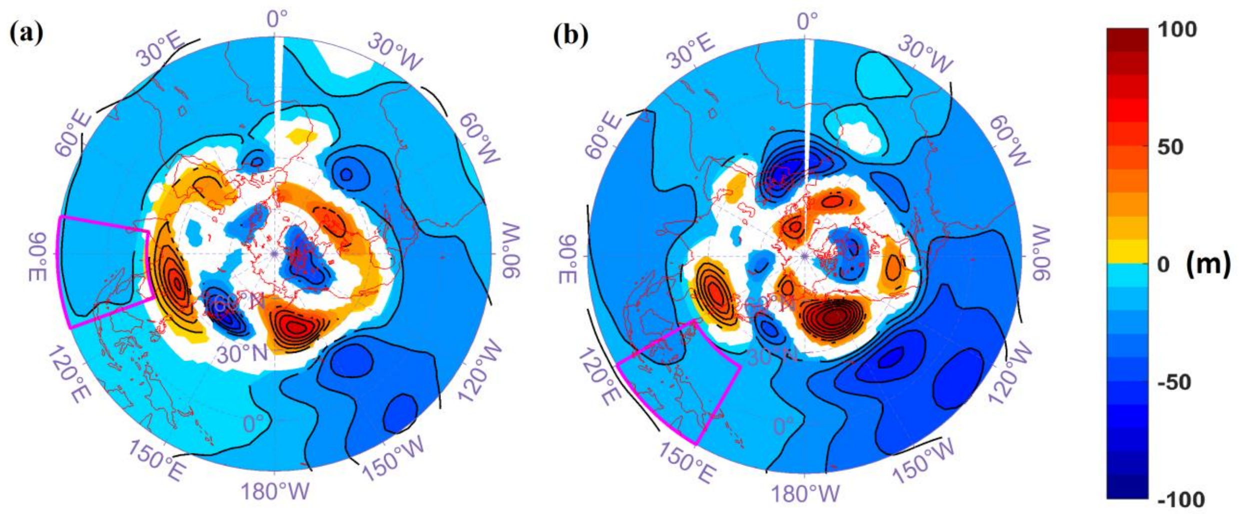

Figure 4: As Fig. 3(a) (forcing over eastern Indian Ocean), but with 250-hPa geopotential height and precipitation from 20-year pre-industrial control integrations of (a) HadGEM2-ES, (b) CCSM4, (c) IPSL-cm5a-MR, (d) GFDL-esm2G, (e) MIROC5 and (f) MPI-esm-MR models, during DJF. Shading is masked out where the step response function is less than one standard deviation, and contour lines are only plotted where the step response function is more than two standard deviations.

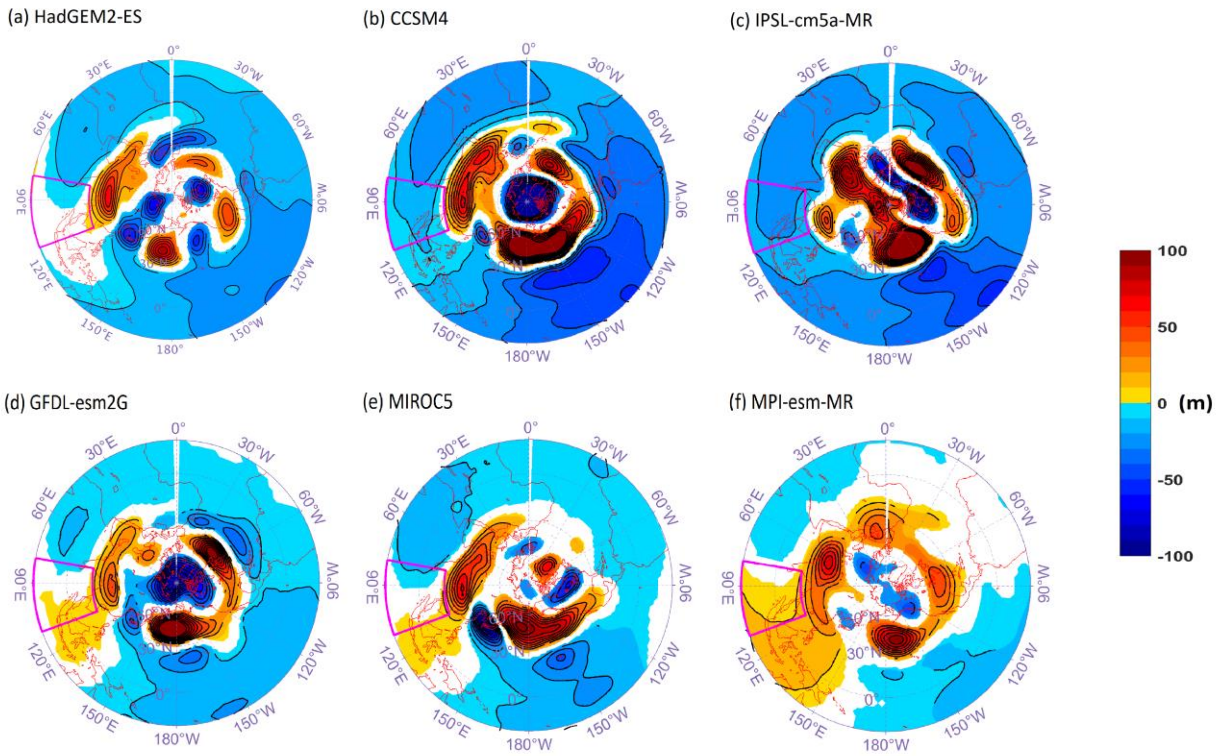

Figure 5: As Fig. 4, but for forcing over the Maritime Continent.

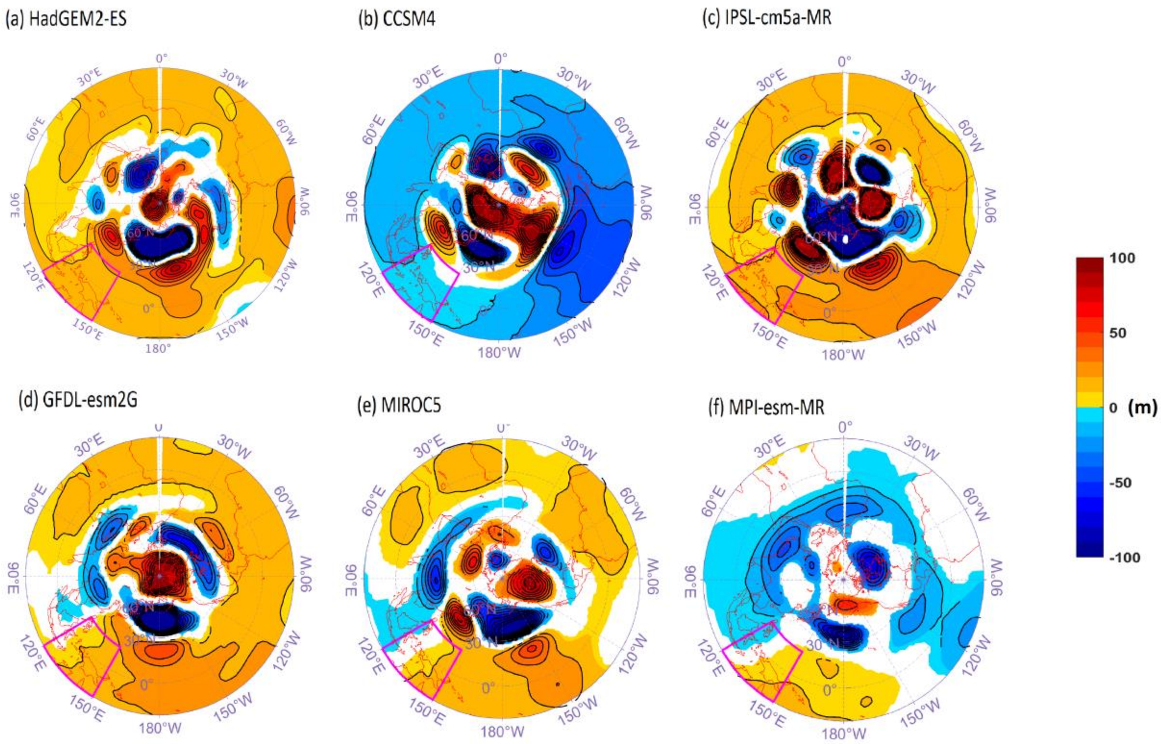

Figure 6: Total stationary wavenumber calculated from winter (DJF) time-averaged zonal wind at 250 hPa for (a) HadGEM2-ES, (b) CCSM4, (c) IPSL-cm5a-MR, (d) GFDL-esm2G, (e) MIROC5, (f) MPI-esm-MR and (g) NCEP/NCAR reanalysis. Black (gray) shading represents regions with negative ū (β*). White contour lines show selected wavenumbers 4 and 5.

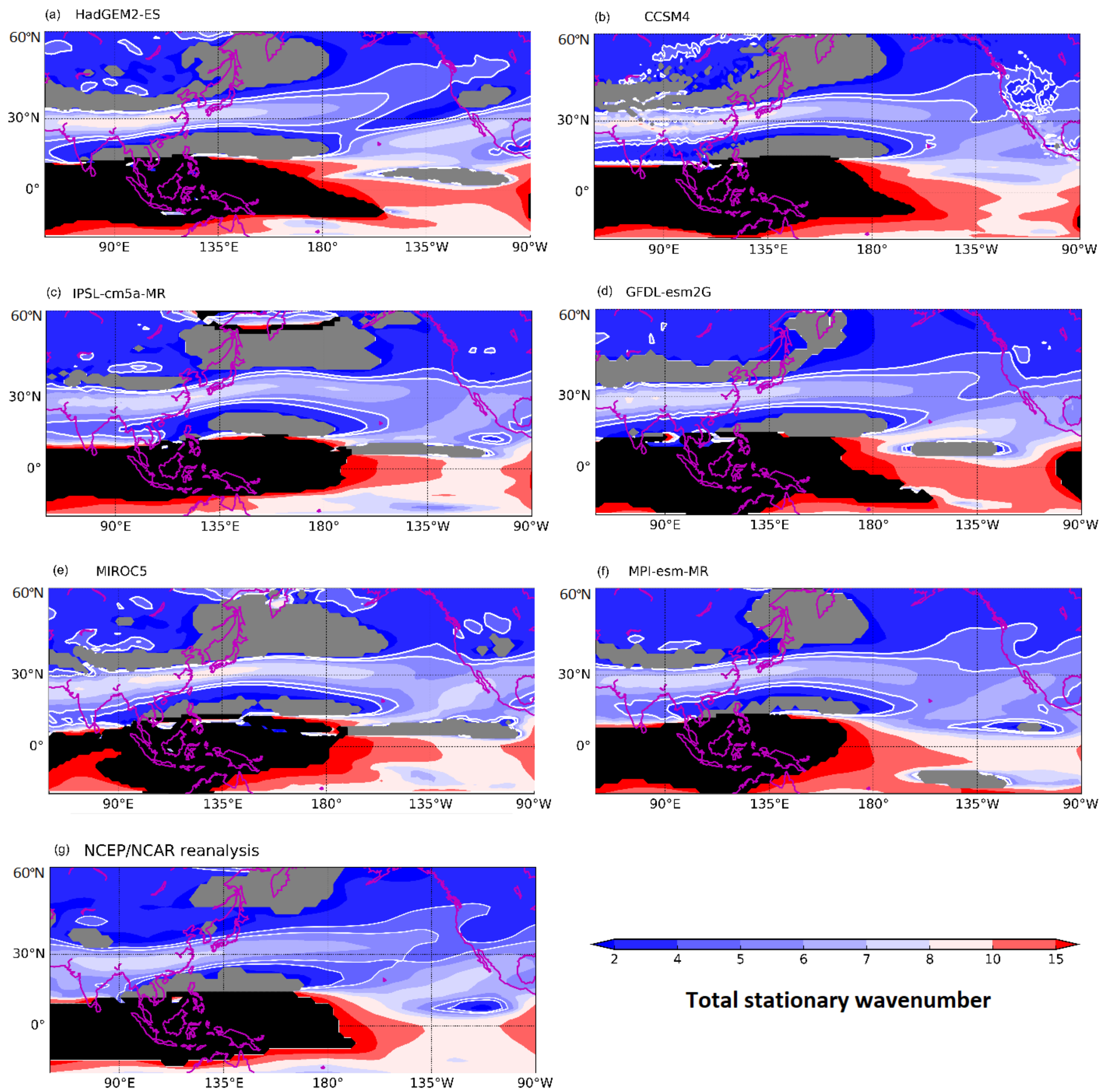

Figure 7: (a) Step response function for anomalous 250-hPa geopotential height from NCEP/NCAR reanalysis, averaged over lag 30-40 days, forced by one standard deviation of the similarity projection metric (for composite DJF precipitation anomalies during El Niño years) calculated from daily TRMM precipitation, over 20 °S - 20 °N, (b) the composite map of anomalous 250-hPa geopotential height from NCEP/NCAR reanalysis during DJF of El Niño years.

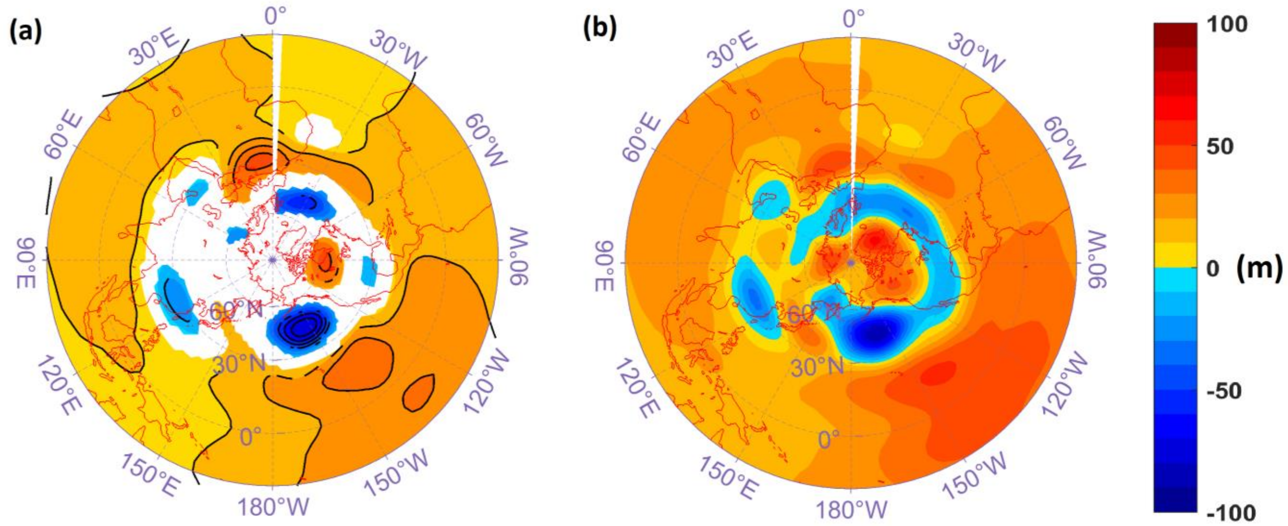

Figure 8: (a) Composite mean of daily TRMM precipitation anomalies over days when the similarity projection metric (see text for details) values were within the upper quartile, from a high emission scenario (RCP 8.5), as simulated by the HadGEM2-ES model. (b) As (a) but for the similarity projection metric calculated from *model* precipitation from the present day simulation. (c) As (b) but for *model* precipitation from the future simulation. (d) Projected changes in mean northern winter (DJF) precipitation (mm day^{-1}) over the future period 2025/26-2045/46 (relative to present day 1986/87-2005/06).

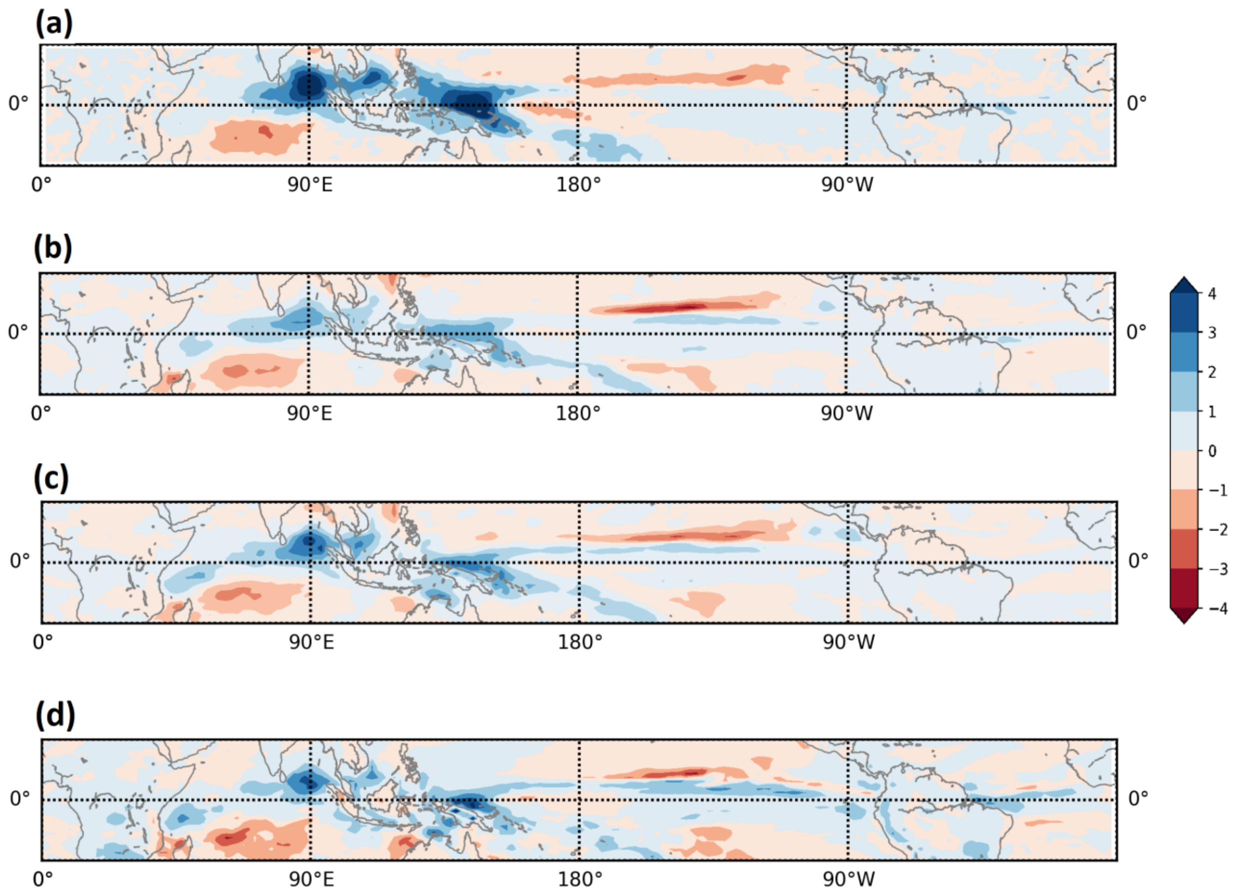

Figure 9: (a) Step response function (m) for anomalous 250-hPa geopotential height from NCEP/NCAR reanalysis, averaged over lag 30-40 days, forced by one standard deviation of the similarity projection metric (for the pattern of future tropical precipitation change *x*) projected onto daily TRMM precipitation $\boldsymbol{y}(t_j)$ during the period DJF 1998/99-2017/18 (Fig. 8a). (b) As (a) but for 250-hPa geopotential height from HadGEM2-ES, forced by the similarity projection metric calculated from daily present HadGEM2-ES model precipitation during the period DJF 1986/87-2005/06 (Fig. 8b). (c) As (b) but forced by the similarity projection metric calculated from daily future model precipitation HadGEM2-ES model precipitation during the period DJF 2025/26-2045/46 (Fig. 8c). (d) Projected changes in average winter (DJF) 250-hPa geopotential height over the period 2025/26-2045/46 (relative to 1986/87-2005/06) from a high emission scenario (RCP 8.5), as simulated by the HadGEM2-ES model. Shading is masked out where the step response function is less than one standard deviation, and contour lines are only plotted where the step response function is more than two standard deviations.

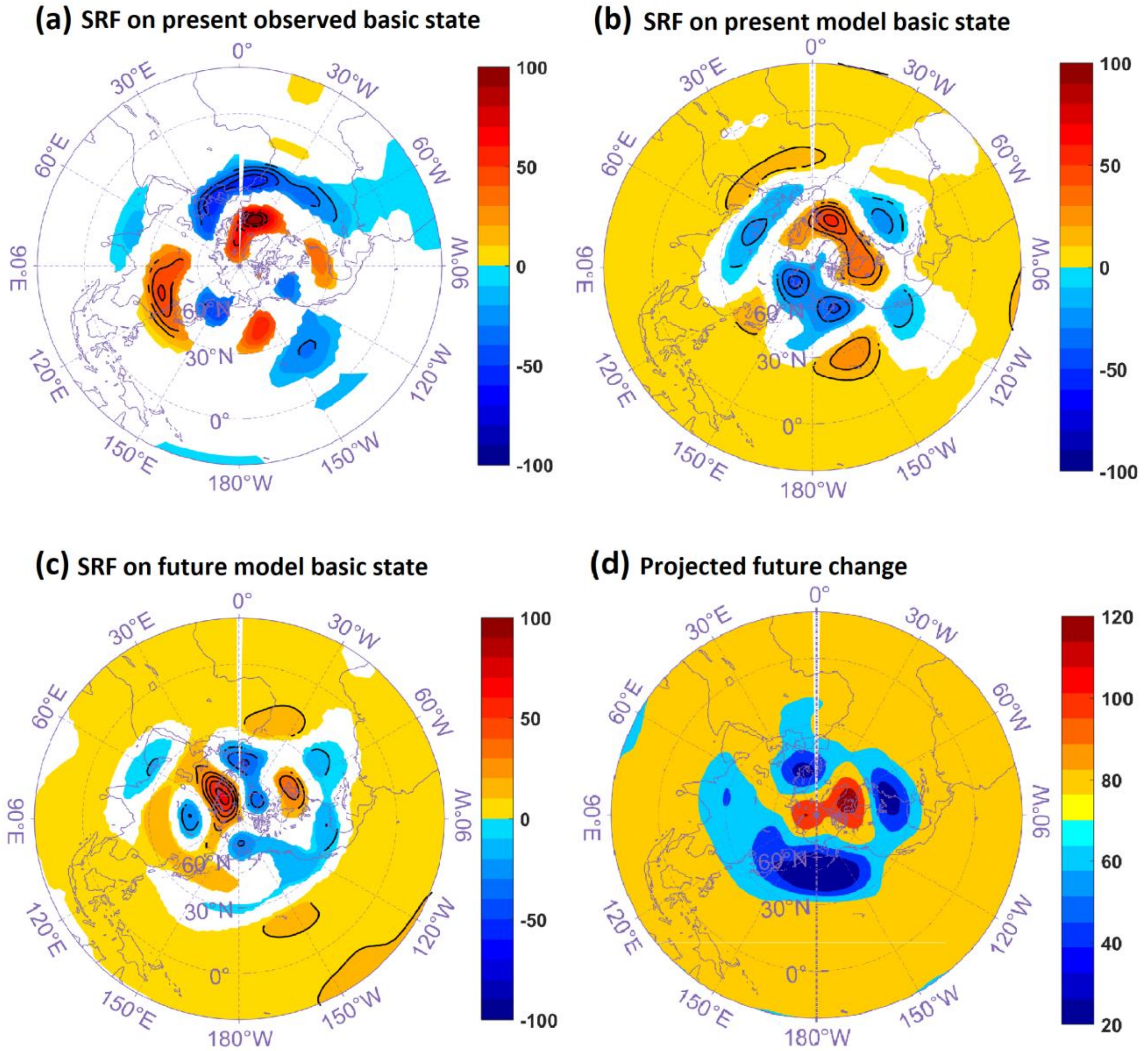
(a) SRF on present observed basic state
(b) SRF on present model basic state
(c) SRF on future model basic state
(d) Projected future change
0°
30°E
30°W
60°E
60°W
90°E
90°W
120°E
120°W
150°E
150°W
180°W
60°N
30°N
100
50
0
-50
-100
120
80
60
40
20